LA-UR-02-4822

Approved for public release; distribution is unlimited.

Title: A Narrow-Gap Ion Chamber for Beam Motion Correction in Proton Radiography Experiments

Author(s): Larry Schultz, Kris Kwiatkowski, Chris Morris, Alexander Saunders, Greg Hart, Gary Hogan, Frank Merrill, Kevin Morley

Submitted to: SIMULATION & ANALYSIS WORKSHOP - PART 1 TOOLS. AUGUST 5-9, 2002
and to
Nuclear Instruments and Methods

Los Alamos
NATIONAL LABORATORY

LA-UR-02-4822

A Narrow-Gap Ion Chamber for Beam Motion Correction in Proton Radiography Experiments

Larry Schultz#, Kris Kwiatkowski, Alexander Saunders, Chris Morris, Greg Hart, Gary Hogan, Frank Merrill, Kevin Morley

Physics Division, Los Alamos National Laboratory

and

#Portland State University

Abstract

The beam illumination pattern, used in proton radiography (pRAD) experiments, displays approximately 2-D Gaussian profile. Typically, the radiographs are normalized to averaged CCD images of the raw beam distribution. However, movement of the beam centroids from pulse to pulse introduces errors in this image normalization process. This paper describes the development, calibration, and use of an ion-chamber beam position monitor (BPM) capable of measuring beam centroid shifts to a few 100μm on pulses spaced less than a microsecond apart.

Introduction

Proton radiography (pRAD) has been demonstrated to be an effective technique for flash radiography of dynamic systems. The technique, developed by collaborators from Los Alamos and Lawrence Livermore National Laboratories, is particularly applicable to dynamic radiography of dense objects. Numerous pRAD experiments have been carried out at the Los Alamos Neutron Science Center (LANSCE) with 800 MeV protons, and at Brookhaven National Laboratory's Alternating Gradient Synchrotron (AGS) with 24 GeV protons.

The pRAD approach offers several advantages over conventional x-ray flash radiography in dynamic experiments. These advantages include inherent multi-pulse capability, high penetrating power, and the ability to tolerate large stand-off distances from the test object for both the incoming and outgoing beam. Additionally, pRAD provides the unique possibility of measuring the density as well as the material composition of a test object with a pulsed system. Details of the technique have been described in [1,2].

A schematic of the LANSCE pRAD setup is shown in Figure 1. The proton beam from the accelerator passes through the diffuser (typically a disk of tungsten of 0.5 mm nominal thickness) at location D. The diffuser introduces divergence in the beam to increase the illumination area. The first magnetic lens focuses the beam on an imaging station (IL0) used for beam monitoring. The second lens focuses the beam on the object at location OL. After passing through the object, the beam passes through a third lens to produce an image at location IL1. Images are formed on a thin (2 mm) LSO scintillator mosaic which acts as a radiation-to-light converter. Images are recorded with an array of seven fast, individually gated CCD's systems [2]. Image-pixel intensity levels are a function of integrated object density along the path of the protons through the object.

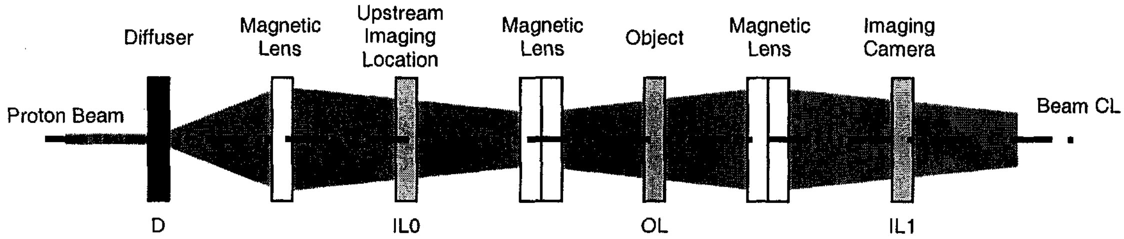

Figure 1 – LANSCE PRAD Beam Line Schematic

An issue that must be dealt with when using accelerator produced beams is non-uniform proton "illumination" of the object. As it arrives at the object location, the proton beam exhibits an approximately 2-D Gaussian intensity profile. In order to "flatten" images taken via illumination with such a non-uniform source, it is necessary to divide the raw images by the corresponding intensity profile of the incoming beam. Unfortunately, there is variability from pulse to pulse in the beam profile, so there is no "standard" beam profile to be used for this purpose.

One method to deal with this problem is to measure online the beam profile, or parameters from which the beam-profile can be reconstructed. This approach was implemented at the Brookhaven National Laboratory AGS accelerator as described in [3,4], wherein single shot CCD cameras and BeO phosphor plates were mounted upstream of the diffuser (no upstream imaging station as shown in Figure 1 (IL0) is available at the AGS). An empirical model was developed to predict the beam profile at the object location from these upstream images. This approach worked well for single pulse imaging, but for dynamic experiments where pulses are often spaced less than 1 μs apart, the single shot CCD's are not suitable.

The beam line configuration at LANSCE allows for a different approach. At LANSCE the upstream imaging location (IL0) is available for direct measurement of the beam profile. A full set of imaging cameras like those at IL1 could be placed at IL0 to measure the beam but this is an expensive approach. Moreover, it has been observed that the LANSCE beam intensity profile is relatively stable, whereas the beam centroid position can on occasion move 1-2 mm from pulse to pulse. A simple, fast beam centroid position monitor (BPM) was developed. The design, calibration, and use of this device in image analysis are described in the remainder of this paper.

Fast Pulse-by-Pulse Hydrogen Beam Position Monitor

An inexpensive alternative to a CCD beam profiler is a fast hydrogen gas ion chamber, which has a multi-pulse capability. A schematic drawing of the detector is shown in Figure 2. The chamber is implemented in simple narrow-gap parallel-plate electrode geometry. The drift gap between the cathode and anode is 0.7 mm. Both electrodes are made of thin copper/gold plated FR-4 boards. The cathode board is 0.8 mm thick with a grounded conductive layer on the outside. The anode board is segmented into a set of inner and outer quadrants. The radius bounding the inner quadrants is 40 mm, and it is70 mm for the outer quadrants. For this experiment only the inner quadrants were used. Because of the compact axial-field geometry (i.e. the field lines are parallel to the beam direction) and because of the fast collection of all charges, there is no Frisch grid. The ion chamber integrates the charge produced by the beam in each quadrant (I_i). The signals from the quadrants are amplified (~10) in a fast amplifier (Phillips NIM 777) and are recorded by a Tektronix RT-720 digitizer. We also observe a small contribution to the signal due to secondary electron emission from the direct interaction of beam protons with the electrodes.

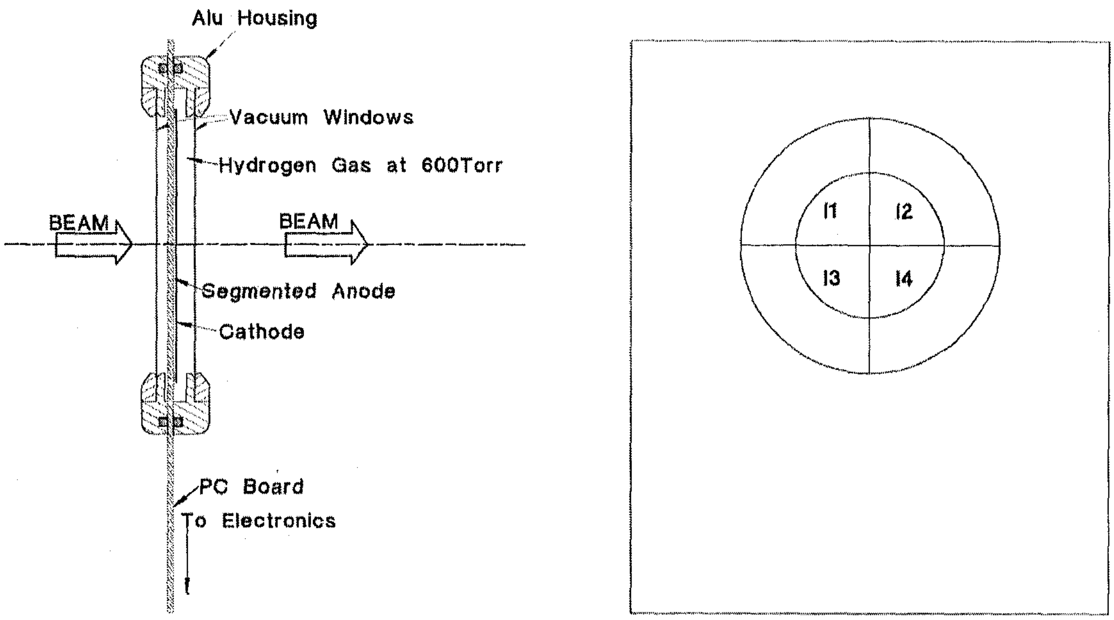

Figure 2 – Schematic view of the cross-section of the ion chamber (left panel; not to scale), and the plan view of the segmented anode (right panel).

The small active gap of the chamber is dictated by the need for the completion of the charge collection before the arrival of the next beam pulse, often within 358ns. The hydrogen gas was selected as the active medium because of is its robustness in response to the high intensity proton beam, and in order to minimize fluctuations due to nuclear reactions of the beam protons with the gas [5,6]. Another advantage of hydrogen is the high mobility of positive H^+ and H_3^+ ions (~13 cm^2/V/s) [7] which is a factor of 5 to 10 higher than for other gases except for Helium. The high ion mobility, small gap, high electric field lead to fast collection of positive ions and minimized the buildup of space charge. The ion chamber functioned well even with high intensity micro-pulses (~6×10^9 protons). For a 60 ns wide beam burst the signal pulse baseline is restored in 200 ns.

Calibration

Relying on the assumption of approximately 2-D Gaussian beam profile, the horizontal (d_h) and vertical (d_v) position of the beam center relative to the center of the detector may be written as:

$$P_v = \frac{I_1 + I_2}{\sum_i I_i}; \qquad P_h = \frac{I_2 + I_4}{\sum_i I_i}$$

$$Z_v = N^{-1}(P_v); \qquad Z_h = N^{-1}(P_h)$$

$$d_v = \hat{S}_v Z_v; \qquad d_h = \hat{S}_h Z_h$$

where N^{-1} represents the inverse of the cumulative standard normal distribution, and $\hat{S}_v$ and $\hat{S}_h$ are free parameters representing the estimated standard deviations of the beam profile at the detector in the vertical and horizontal directions, respectively. These free parameters were adjusted for fitting BPM to image data during calibration.

As was mentioned above, it is standard procedure to take a number of images of the raw beam prior to or after imaging an object. These beam images provide the dataset for calibration. Beam centroids shifts in the beam images were estimated by fitting a 2-D Gaussian profile to each digital beam image. The *I* parameters from the beam position monitor were recorded for the beam pulses which produced each beam image. After transforming the BPM data at IL0 to the *Z* statistics, a linear fit was applied to adjust $\hat{S}_v$ and $\hat{S}_h$. Sample results for horizontal beam shift are shown in Figure 3 with an error analysis in Table I. The resulting resolution was determined to be 187 μm by subtracting the variance due to error in extracting beam shifts from images. This image analysis error was established by analyzing images of several single pulses of which beam images were taken by multiple CCD cameras at IL1.

Table I – Analysis of BPM Error for Horizontal Beam Movement

Source	**Variance, σ_h^2 [mm^2]**	**RMS, c_h [mm]**
Beam movement extracted from images	.329	.574
Residual from BPM→Image Fit	.038	.194
Estimated error in extracting beam movement from image analysis	.003	.050
Estimated BPM→Real beam movement error	.035	**.187**

Vertical beam movement from the LANSCE accelerator turned out to be quite small (as expected), with a vertical beam shift of 0.143 mm RMS as extracted from the images. There was essentially no correlation between the BPM and images for the small vertical shifts, not surprising since the vertical shift was less than the overall resolution of 0.187 mm.

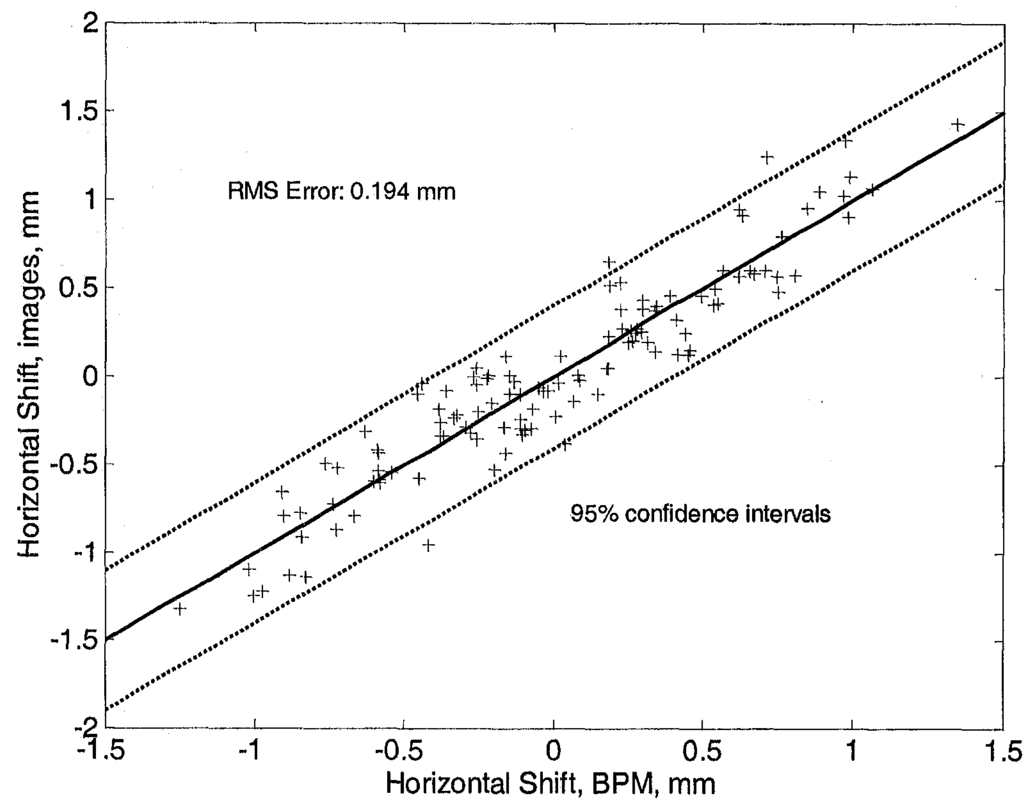

Figure 3 – Results of BPM calibration process for horizontal beam shift.

Image Analysis

To apply beam shift data from the BPM, we could spatially shift the pixels in an image by the appropriate amount before dividing. However, this procedure would erroneously move fixed pattern noise as well. Instead, we apply the correction by adjusting the pixel gain of an image I, given a desired shift (d_x, d_y) as:

$$I_{corr}(x,y) = I(x,y) \cdot e^{-\left[\frac{x^2-(x-d_x)^2}{2\sigma_x^2}+\frac{y^2-(y-d_y)^2}{2\sigma_y^2}\right]}$$

The values of the σ range from 20 to 38mm, with 25mm being typical. Images from a recent pRAD experiment are shown in Figure 4. The object is barely visible due to non-uniform illumination. The grid and Moiré patterns in the images are artifacts of the CCD image capture system. Flattening the object image by dividing by the beam images substantially reduces this fixed pattern noise while also producing more uniform illumination of the object.

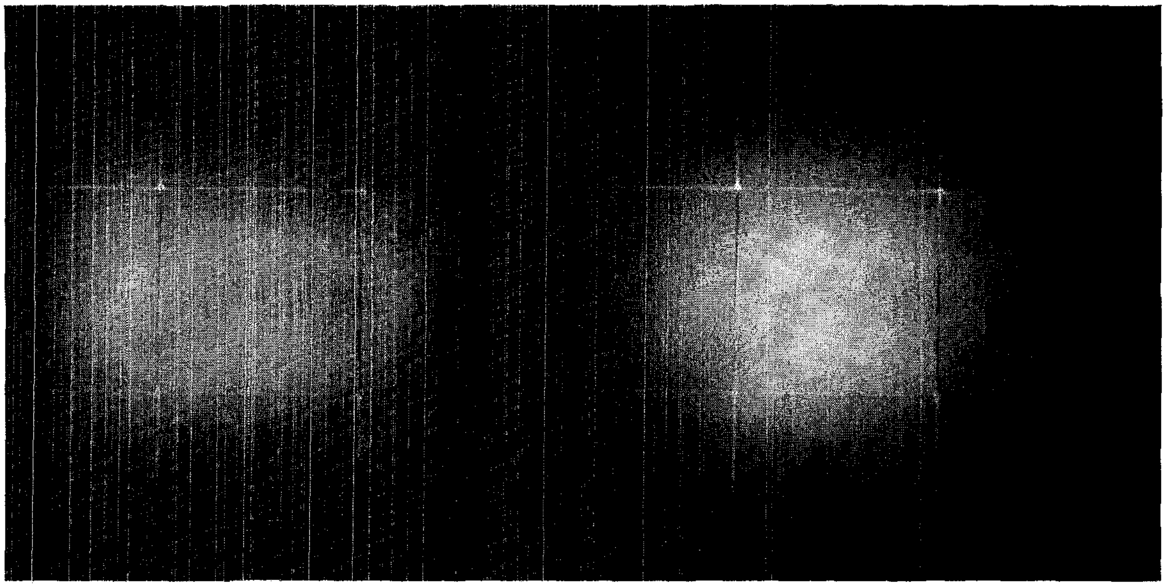

Figure 4 -- Object (left frame) and beam (right frame) images from a recent PRAD experiment.

Shown in Figure 5 are images produced by dividing the object image by the beam image, with and without BPM correction. The object is now clearly visible and fixed pattern noise is greatly reduced. However, it is apparent in the uncorrected image that the background area is darker on the left side of the object than on the right side. This effect was caused by horizontal beam movement, resulting in a different position of the beam when the object and beam images were taken. Although the effect is most noticeable in the background, the more serious problem is that apparent density of the object itself is skewed.

The corrected image was produced by applying the BPM adjustment to both the object and beam images, then dividing the adjusted object image by the adjusted beam image. The improved uniformity of the background is apparent. For a simple quantification of the results, we project the image onto the horizontal coordinate and extract the RMS pixel value in the background area of the projection. For the uncorrected image this metric has a value of 0.161, and for the corrected image the value is 0.011. This represents a 93% reduction in the background non-uniformity.

When BPM was not available the error due to pulse to pulse beam movement has been mitigated by using an average of several beam pictures instead of just one. Also, if the object being radiographed does not fill the field of view (as is the case in this example), the pattern of non-uniformity extracted from the background can be used to analytically flatten the final images. This is at best a tedious manual procedure, however, and impossible to apply in many PRAD experiments where the object fills the field of view.

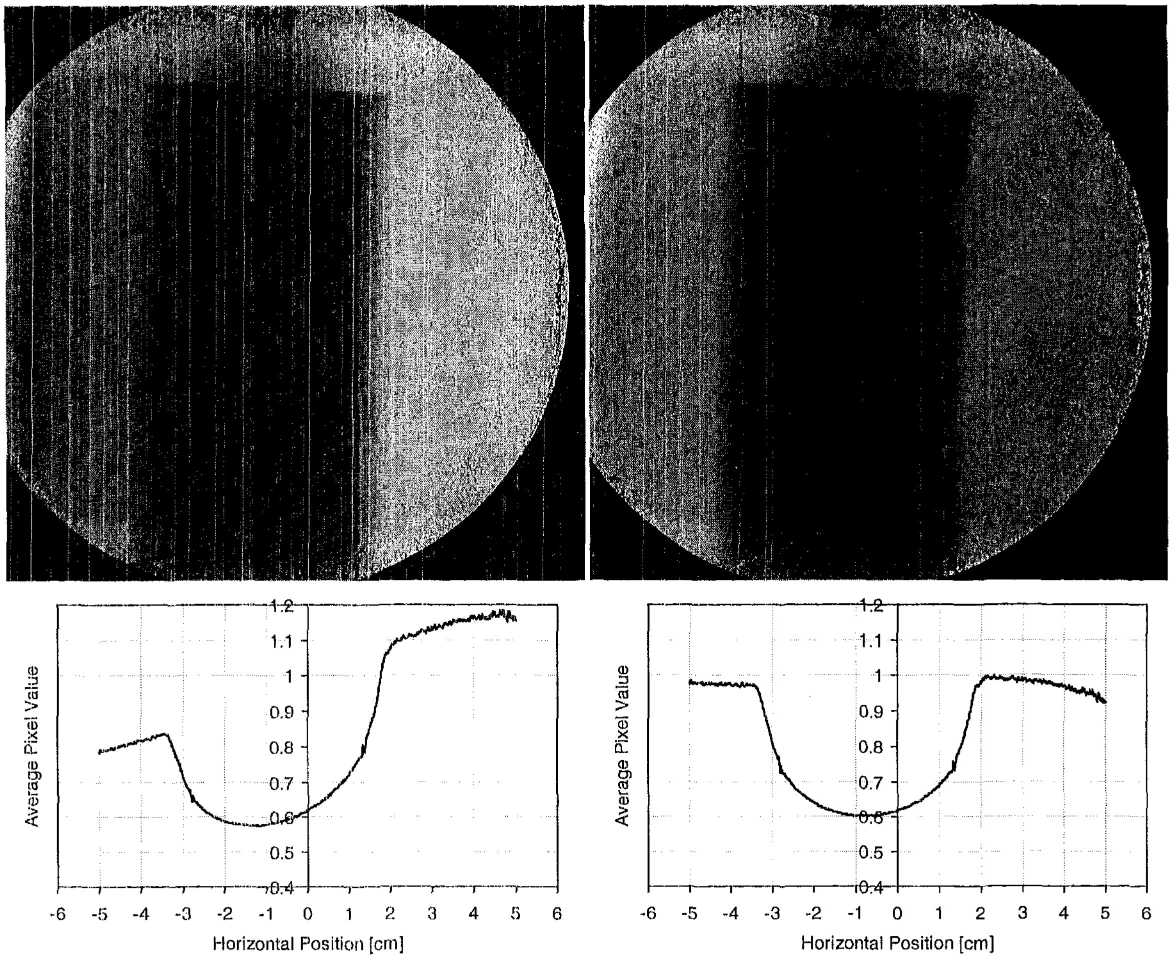

Figure 5 – Comparison of image flattening with (left) and without (right) use of BPM data. Projected pixel density along the horizontal coordinate is shown in the lower frames.

Summary

The hydrogen beam position monitor has proven to be an effective, low cost means for measuring beam position to feed PRAD image correction. An extra imaging station is available at the LANSCE PRAD station for the BPM, but in principle such a detector could be placed at any available location between the diffuser and the object. Hence the hydrogen BPM is a candidate for beam position monitoring at other or future PRAD implementations.

Acknowledgements

The authors gratefully acknowledge the technicians, engineers and scientists of the LANL Proton Radiography Team, as well as the LANSCE facility, Los Alamos National Laboratory and the U. S. Department of Energy for enabling this effort.

References

[1] Morris, C. L. and J. D. Zumbro, "Overview of Proton Radiography – Concepts and Techniques," Technical Report LA-UR-97-4172, Los Alamos National Laboratory, 1997.

[2] King, N.S.P., et al., "An 800-MeV Proton Radiography Facility for Dynamic Experiments," *Nuclear Instruments & Methods in Physics Research A*, **424** (1999), pp 84-91.

[3] Morris, C. L. and E. P. Hartouni, "Proton Radiography at the AGS in the U-line," Technical Report AGS Proposal 955 / LA-UR-00-4797, Los Alamos National Laboratory, 2000.

[4] Wohlberg, B. E., et al., "Initial Beam Profile Modeling for BNL AGS Experiment 955," Technical Report pending publication, Los Alamos National Laboratory, 2002.

[5] Bowman, J. D., et al "Low Noise Ionization Chambers for Use in Transmission Measurements with Medium and High Energy Beams", *Nuclear Instruments and Methods* **216** (1983), pp 399-404.

[6] Kwiatkowski, K., et al., "Development of Multiframe Detectors for Ultrafast Radiography with 800 MeV Protons," *IEEE Transactions on Nuclear Science,* **49** (2002), pp 293-296.

[7] Simko, T., et al., "Computer Simulations of H^+ and H_3^+ Transport Parameters in Hydrogen Drift Tubes", *Physical Review E*, **56** (1997), pp 5908-5918.